2009 American Control Conference
Hyatt Regency Riverfront, St. Louis, MO, USA
June 10-12, 2009

Design and Relay-Based Control of a Novel Linear Magnetostrictive Motor

Won-jong Kim, *Senior Member, IEEE, Member, ASME,* and Ali Sadighi, *Student Member, IEEE*

***Abstract*—Design and relay-based control of a novel linear magnetostrictive motor is presented in this paper. The magnetostrictive material used here is Terfenol-D, an alloy of the formula $Tb_{0.3}Dy_{0.7}Fe_{1.9}$. In response to a traveling magnetic field inside the Terfenol-D element, it moves in the opposite direction with a peristaltic motion. The proposed design offers the flexibility to operate the motor in various configurations including local and conventional three-phase excitation. In this paper, we demonstrate that the power consumption can be reduced significantly by the local-excitation approach. A new force transmission assembly incorporates spring washers to avoid the wear due to its sudden collision with the Terfenol-D element. The closed-loop control system was implemented using relay control which resulted in an optimal closed-loop performance. The magnetostrictive motor has demonstrated 410-N load capacity with a travel range of 45 mm, and the speed is around 9 mm/min currently. The low speed is due to the local three-phase operation mode, and it could be increased to 60 mm/min by using the conventional three-phase operation. The maximum power consumption by the motor is 95 W.**

I. Introduction

Linear electric motors have found many industrial applications and are extensively used in precision manufacturing automation, textile sewing machines, free piston pumps and compressors, etc. [1]. However, there are key applications which impose limits on the space required for the actuator or its power consumption. Meeting all these requirements is a challenging task which pushes us to explore new technologies for the development of such actuators [2]. Hydraulic motors, despite their high-force-generating capability, are not applicable where ample space is unavailable to accommodate the auxiliary parts of the hydraulic system such as a hydraulic pump, etc. On the other hand, direct-drive linear electric motors could not compete with hydraulic ones in generating high forces, so rotary motors have been combined with gear reducers and ball or lead screws to increase the force capability. This approach, although effective in many situations, requires the added complexity of a speed reducer and introduces backlash.

Considering these limitations, attentions have been paid to smart materials as a new approach to develop novel actuators. Among them, giant magnetostrictive materials are in competition with piezo ceramics [3]. The magnetostrictive materials have found their place in specific applications such as low-voltage, high-force actuators, high-power low-frequency transducers, and space cryogenic positioning. In other cases piezo-ceramic actuators are employed because of their low-power consumption and high-output energy per mass unit [4].

Terfenol-D, an alloy of formula $Tb_{0.3}Dy_{0.7}Fe_{1.9}$ was developed in the 1950's at the Naval Ordnance Laboratory. This alloy has the highest magnetostriction of any alloy, up to 2000 ppm [5]. Due to this small magnetostriction strain level, most of the available magnetostrictive actuators are capable of generating high forces within a very small range of actuation. One of the first studied applications of these materials was as a generator of force and motion for underwater sound sources [6]. The first type of extended-range magnetostrictive motors was developed by Kiesewetter [7]. He conceived of the idea of generating the peristaltic motion with a Terfenol-D rod in a tight-fitting tube. The main drawback of his motor is wear, which would cause a loose contact between the Terfenol-D rod and the tube, leading to the loss of its force-generating capability.

To overcome this problem Kim, et al. constructed an extended-range linear magnetostrictive motor with double-sided three-phase stators [8]. Unlike the Kiesewetter motor, they used Terfenol-D slab placed between two tight-fitting plates spring-loaded to maintain proper contact in spite of wear, thermal expansion, or motion. They demonstrated force generating capability up to 140 N and a travel range of 25 mm. However, the power consumption was high due to applying conventional three-phase excitation in high frequency which gave rise to eddy-current loss [9].

We have developed a new type of linear magnetostrictive motor with a rectangular slab of Terfenol-D as the active element as shown in Fig. 1. To overcome the power consumption limitation, we designed and implemented a novel configuration for coils. In this motor, the coils' magnetic axis coincides with the active element's magnetic axis, which aligns the direction of magnetic field inside the Terfenol-D slab better and results in higher magnetic flux density and consequently higher magnetostrictive strains. Furthermore, this design enables us to implement various operation modes such as the conventional multi-phase excitation or a local multi-phase excitation. The main focus of this paper is the local three-phase operation of the linear magnetostrictive motor. Since only three out of twenty-four coils are excited at each time in this operation mode, the power consumption could be cut drastically. To date, we demonstrated a speed of 9 mm/min with a 410-N load capacity with a 45-mm travel range.

Won-jong Kim and Ali Sadighi are with the Department of Mechanical Engineering, Texas A&M University, College Station, TX 77843-3123, U.S.A. (Email: wjkim@tamu.edu, a_sadighi@tamu.edu)

978-1-4244-4524-0/09/$25.00 ©2009 AACC

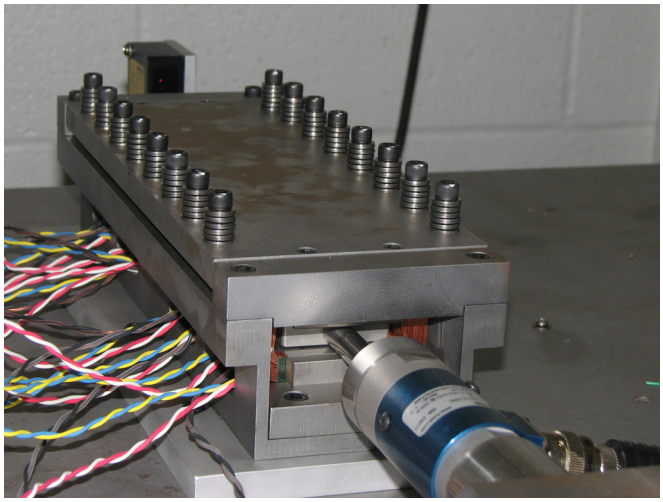

Fig. 1. Photograph of the linear magnetostrictive motor.

In the next section, we present the working principle and electromagnetic design of the linear magnetostrictive motor. Its mechanical design and fabrication is discussed in Section III. Section IV describes the power electronics and control system. Open-loop and closed-loop test results are then presented and discussed in Section V.

II. Working Principle and Electromagnetic Design

The working principle of the linear magnetostrictive motor is depicted in Fig. 2. The main idea is to generate a traveling magnetic field inside the active element while keeping it under pressure. The active element is initially at rest in a tight fit inside a channel. A magnetic field could be generated by the means of coils surrounding the active element. A pair of stators as shown is incorporated to enhance the magnetic flux density inside the active element. Now if we move this magnetic field to the right, as it comes to interaction with the active element, it makes its portion elongate along the magnetic field lines. Since its volume is constant, this elongation will result in cross-sectional contraction which releases the active element from its tight fit with the channel. As the magnetic field moves to the right, the neighboring portion of active element expands while the last portion goes back to its original place and locks against the channel. When the magnetic field has passed completely through its length, the active element has moved to the left. By repeating this process over and over, this peristaltic motion results in overall displacement of the active element.

A. Underlying Theory

It has been shown that the speed of a linear magnetostrictive motor is a function of peak magnetostrictive strain, mechanical stress, and operation frequency [10]. For the linear magnetostrictive motor with local multi-phase operation, the modified relationship between the motor speed and design parameters is given by:

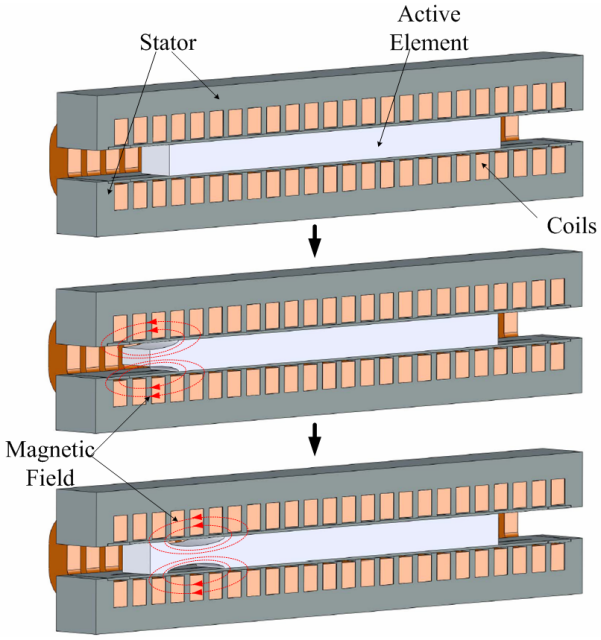

Fig. 2. Working principle of linear magnetostrictive motor. By generating a traveling magnetic field through the active element, the so-called peristaltic motion is generated which results in overall displacement of the active element to the opposite direction of the traveling magnetic field. The size of the bumps due to magnetostriction is exaggerated for clarity.

$$v = N f p \left(\varepsilon_{\max} - \frac{F}{EA_T}\right), \quad (1)$$

where

N Number of phases (3)
f Local multi-phase operation frequency (Hz)
p Slot pitch (10.9×10^{-3} m)
$\varepsilon_{\max}$ Peak magnetostrictive strain under no-load condition
F External load (N)
E Young's modulus of Terfenol-D (35×10^{9} Pa)
A_T Cross-sectional area of the Terfenol-D slab (400 mm^2)

Thus, the speed of the magnetostrictive motor relates to the superposition of opposing strains from two different origins. One is the magnetostrictive strain denoted by $\varepsilon_{\max}$, and the other is mechanical strain denoted by F/EA_T resulted from the external load applied on the motor.

B. Electromagnetic Design

As seen above, the magnetostrictive strain has a direct impact on the speed and force capacity of the linear magnetostrictive motor. Hence, the main issue of the magnetic circuit design is to direct the magnetic flux as much as possible through the active element, which would lower the power requirements as well as to increase the force capacity. We employed a finite-element-analysis (FEA) approach for the design and optimization of the magnetic circuit [11], [12]. Five different configurations for the key components such as stators, coils, and active element were proposed, and the FEA was run for each configuration.

Finally, by taking into account other design considerations such as ergonomics, ease of manufacturing and assembly, a flat design with single set of coils was chosen.

The eddy-current analysis was carried out for the frequencies of as low as 0.1 Hz up to 60 Hz. After performing the FEA, the core losses were evaluated by integrating the ohmic losses over the volume of the stator and the Terfenol-D slab. It is seen that the core losses will be quite low in this range of frequencies and the need for laminated stators could be eliminated. Optimization of motor parameters was carried out using FEA, in which the coil geometry, number of turns, slot size, and Terfenol-D geometry were optimized. Due to the open-slot geometry, it is possible to use pre-made coils. We incorporated 24 coils each consisting of 273 turns of AWG #24 wire. The proposed design gives us the flexibility to connect these coils in various ways such as two-, three-, or four-phase configurations. Table I summarizes the optimized parameters for the linear magnetostrictive motor.

TABLE I
OPTIMIZED PARAMETERS FOR THE LINEAR MAGNETOSTRICTIVE MOTOR

Item	Specification
Terfenol-D element	31.5 × 12.7 × 200 mm
Number of coils	24
Wire size	AWG #24
Number of turns per coil	273
Coil resistance	4.28 Ω
Coil inductance	9.7 mH
Stator material	Nickel-Iron Alloy 49
Number of slots per stator	24
Slot pitch	10.9 mm
Slot Depth	11.2 mm

III. MECHANICAL DESIGN AND FABRICATION

A characteristic feature of magnetostrictive devices is that the resulting strains are on the order of hundredths to tenths of millimeters. Therefore, special attention must be paid to tolerances in the construction. There is a need to manufacture or machine the magnetostrictive material transmission parts with a tolerance level within a couple or tens of micrometers to achieve predictable performance. It is also important that all surfaces that transmit force and strain are flat and smooth. The smoothness requirement is normally within a couple of micrometers [13]. The mechanical design tasks involve the design of a suitable housing, force transmission assembly, squeezing mechanism, stators and load unit.

A. Housing

The housing was designed considering the external load as well as the squeezing force which are transmitted to the housing structure. To remove the concerns about thermal distortion due to brazing or lack of precision in assembly, we machined the whole structure out of a solid piece of steel A36. The housing is shown in Fig. 3(a).

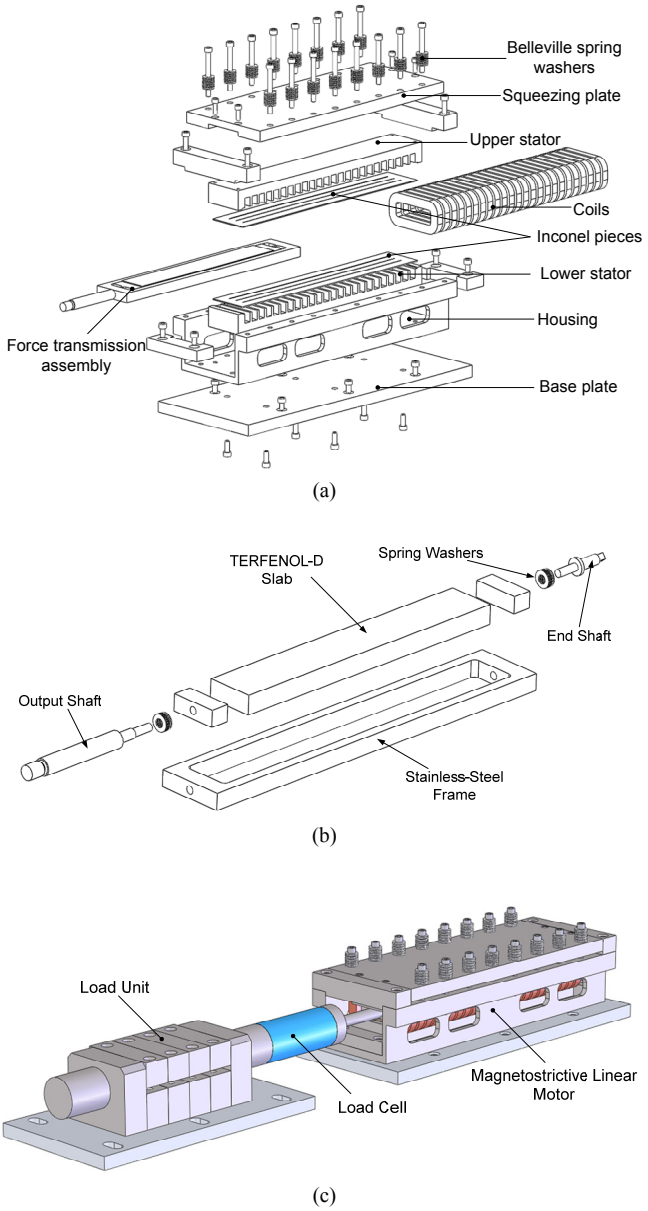

Fig. 3. (a) Exploded view of linear magnetostrictive motor. (b) Exploded view of force transmission assembly. (c) Experiment setup.

B. Stator

The stator in our design should have two main features. First, it should own high relative permeability to decrease the reluctance of magnetic circuit. Second, it should be strong enough to stand the shear forces due to external load as well as the pressure due to squeezing force. To meet these two criteria, we chose Nickel-Iron Alloy 49 (EFI 50 by Ed Fagan), which has very high relative permeability up to 100,000 along with good mechanical properties like yield stress of 154 MPa. Furthermore, a clearance of 0.5 mm is considered between the bottom of stator slots and the coil to avoid the coils' damage due to the normal squeezing pressure. As discussed earlier, we decided to make the stator by machining due to low core losses in low frequencies. The stators are shown in Fig. 3(a).

C. Force-Transmission Assembly

The rectangular slab of Terfenol-D is sandwiched between two stators which are capped with thin pieces of Inconel-718. These thin pieces have very smooth surfaces with the surface roughness of 1 μm, which increase the friction force between the Terfenol-D and the Inconel-718 pieces. These friction forces contribute to the reaction force required to move the active element against a load or to hold it in place. The relative permeability of Inconel-718 (Sheet 718 by Rolled Alloys) is as low as 1.001 which directs most of the magnetic flux through the active element. Since Terfenol-D is very brittle material, making holes or tapping would put it at risk. Hence, we designed a force transmission assembly consisting of a stainless-steel frame surrounding the Terfenol-D. This assembly is shown in Fig. 3(b). The generated force is transmitted to this frame through two rectangular ground pieces of stainless steel. Two sets of spring washers incorporated at each end assure a permanent contact between the Terfenol-D slab and these pieces. It also allows the expansion of Terfenol-D in the longitudinal direction.

D. Squeezing Mechanism

To generate the required friction force between the Inconel-718 pieces and the Terfenol-D element, there should be a normal force applied to this assembly. This normal force is generated using 16 sets of Belleville washers and screws and transmitted through the squeezing plate as shown in Fig. 3(a).

E. Load Unit

The load unit, shown in Fig. 3(c), is a friction-based load. It consists of a ground stainless-steel shaft and four pairs of semicylinders which could be pushed against the shaft using eight hex-head screws, to increase the load force. To be able to measure the load, a load cell is connected to the output shaft of the motor from one end and to the stainless-steel shaft of the load unit on the other end.

IV. Power Electronics and Control System

A. Power and Control Electronics

As mentioned earlier, the proposed design enables us to operate the linear magnetostrictive motor in various configurations including three-phase conventional operation and local multi-phase operation. Here, we focus on local three-phase operation.

The objective of power electronics here is to direct the required current to three adjacent coils and then move it to either side depending on the motor's motion direction. To achieve this goal we designed and implemented three switching boards, each including eight power MOSFETs (model IRF3315Pbf by International Rectifier), eight MOSFET drivers (model TC4420 by Microchip), eight flyback diodes (model MUR405 by ON Semiconductor), three inverters and one 3-line-to-8-line decoder. There is a dedicated power supply (model E3644A by Agilent) for each phase which also monitors the voltage and current of each phase. The schematic view of switching board for one phase is shown in Fig. 4(a), and the switching boards are depicted in Fig. 4(b).

The switching frequency of the power MOSFETs is controlled using the digital inputs/outputs (I/Os) of a digital-signal-processing (DSP) board (model DS1104 by dSPACE). This DSP board is a 32-bit 250-MHz floating point DSP, with eight analog-to-digital (A/D) channels, eight digital-to-analog (D/A) channels, and twenty digital I/O channels. The motor shaft position is monitored with a laser distance sensor (model OADM 20I6460/S14F by Baumer Electric) which has a resolution of 5 μm and measuring distance range from 30 mm to 130 mm. To measure the motor load we use a load cell (model LCB400 by Futek Advanced Sensor Technology) with 4448-N load capacity. Both position and load measurements are fed to two channels of the 16-bit D/A converter of the DSP board. The output voltage of the load cell is amplified and filtered by a differential preamplifier (model ADA400A by Tektronix) before being sent to the D/A converter.

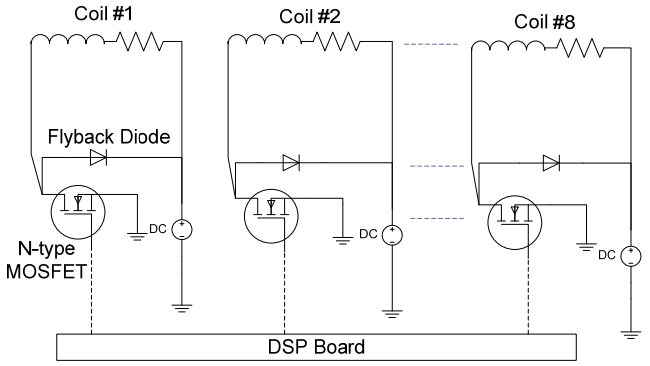

(a)

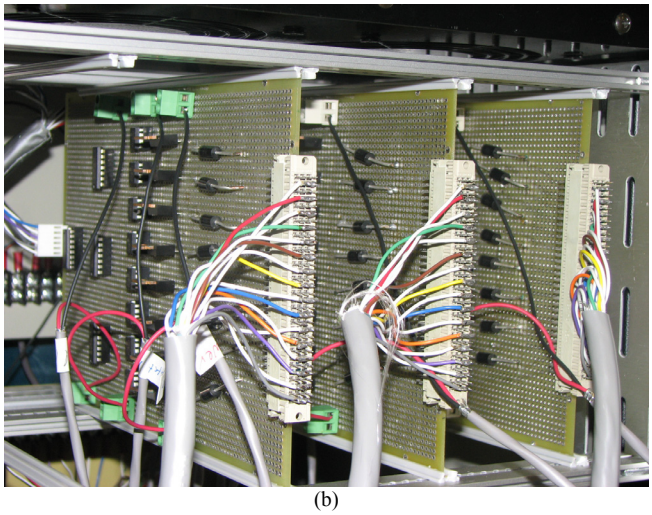

(b)

Fig. 4. (a) Schematic view of a switching board for one phase. (b) Photograph of the switching boards.

B. Open-Loop Tests

Various open-loop no-load tests were carried out at a constant frequency of 10 Hz. As mentioned earlier, this linear magnetostrictive motor was designed to work at low frequencies. Although we sacrifice the speed by operating the motor at low frequencies, its overall efficiency increases due to the reduction in core losses. In Fig. 5, the open-loop no-load motion profiles at the excitation frequency of 10 Hz and with varying peak phase currents from 0.6 A to 2.55 A are shown. As the phase current increases, the profiles get closer to each other, which is due to the saturation inside the active element. The open-loop load test was performed at a phase peak current of 2.75 A and an excitation frequency of 5 Hz. The load was increased from 50 N to 300 N and the motion profiles are shown in Fig. 6. As the load increases, the motor speed decreases, which was predicted by (1).

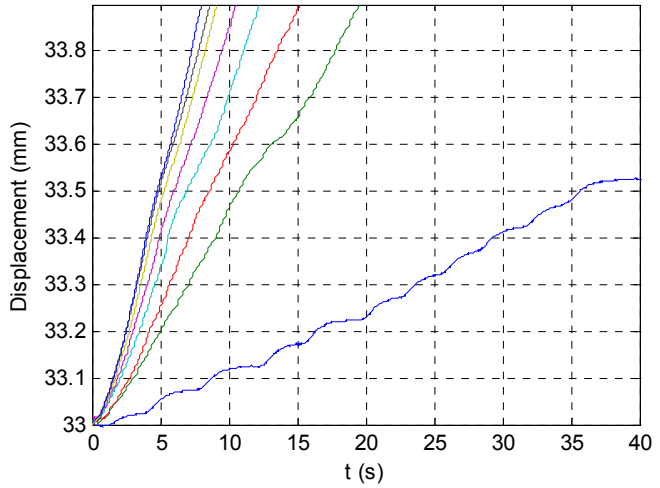

Fig. 5. Open-loop no-load tests of linear magnetostrictive motor excited at 10 Hz and with varying peak phase currents 0.6, 1.1, 1.35, 1.6, 1.85, 2.1, 2.3, and 2.55 A from the bottom.

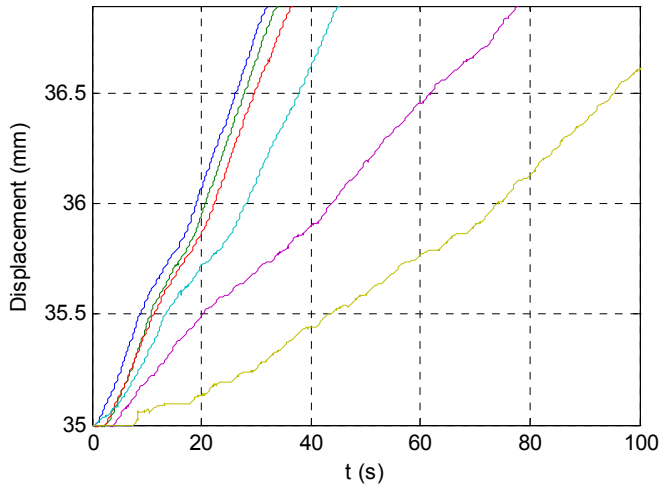

Fig. 6. Open-loop load tests of the linear magnetostrictive motor at the peak phase current of 2.75 A and the frequency of 5 Hz with varying loads 50, 100, 150, 200, 250, and 300 N from the top.

The power consumption of the linear magnetostrictive motor could then be calculated by integrating the current profile and using the following equation:

$$P = NV\left(\frac{1}{T_2 - T_1}\int_{T_1}^{T_2} i(t)\,dt\right) \tag{2}$$

where N is the number of coils, V is the phase voltage, and $i(t)$ is the instantaneous current in each coil.

The maximum power consumption then is calculated at the phase voltage of 13 V as:

$$P = 24\times 13\times\left(\frac{1}{T_2 - T_1}\int_{T_1}^{T_2} i(t)\,dt\right) = 95\ \text{W} \tag{3}$$

V. Closed-Loop Control

We designed and successfully implemented a relay-based control system resulting in the minimum settling time with minimum overshoot. The schematic diagram of the closed-loop control system is shown in Fig. 7.

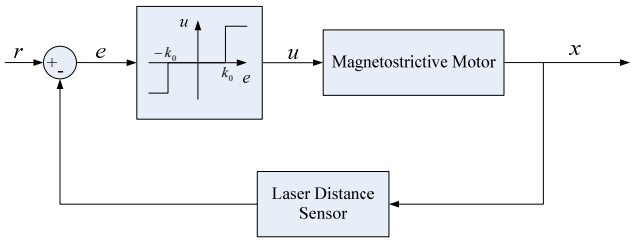

Fig. 7. Schematic diagram of closed-loop control system.

To avoid self-oscillations [14] in the system response, we consider a relay controller with a dead zone defined as:

$$u = \Phi(e) = \begin{cases} +1 & e > k_0 \\ 0 & -k_0 < e < k_0 \\ -1 & e < -k_0 \end{cases} \tag{3}$$

where, the threshold values, $\pm k_0$, define the dead zone of the relay element. By this control law, the absolute value of the control signal is always maximized, which makes the motor move in either direction with the maximum speed. We performed the closed-loop tests with various values for k_0. As seen in Fig. 8(a), for threshold value equal to 0.005 mm, the 1-mm closed-loop step response exhibits self-oscillation. We gradually increased the threshold value, and the self-oscillation frequency decreased as the threshold value increased. Finally, by choosing threshold value as 0.02 mm, the self-oscillation was eliminated. The 1-mm closed-loop step response with the dead-zone threshold value equal to 0.02 mm is shown in Fig. 8(b). There is no more oscillation in the response. By further increasing the threshold value we may even remove the overshoot, but the downside would be the increase in steady-state error. Fig. 8(c), shows the capability of the designed controller in tracking a sinusoidal reference input with an amplitude of 0.5 mm and frequency

of 0.05 rad/s.

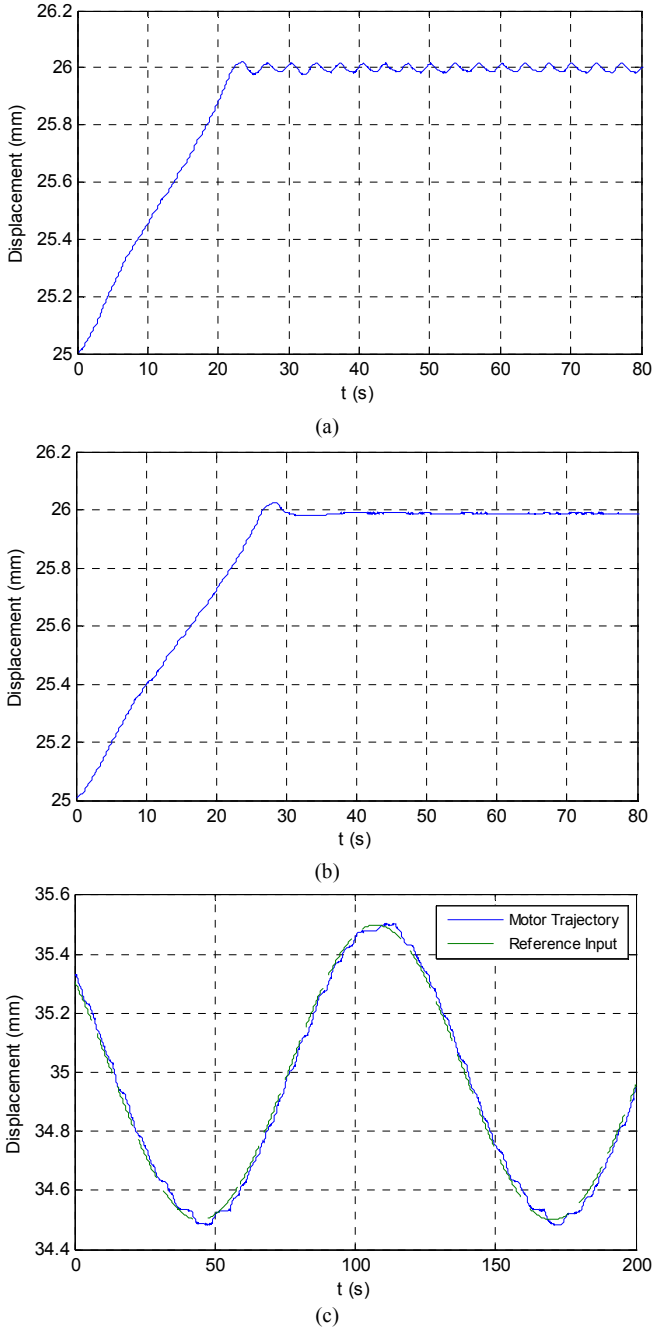

Fig. 8. (a) 1-mm closed-loop step response with an excitation frequency at 10 Hz and a phase voltage of 5 V and the dead-zone threshold values of ±0.005 mm. (b) The same step response with the dead-zone threshold values of ±0.02 mm. (c) Closed-loop response to a sinusoidal reference input with an amplitude of 0.5 mm and frequency of 0.05 rad/s.

VI. Conclusions

We designed and implemented a low-power linear magnetostrictive motor. An FEA tool was used to design and optimize the magnetic circuit of the magnetostrictive motor. Our design allowed the flexibility to operate the motor in various configurations depending on the type of applications. A local three-phase operation mode was developed in response to the requirements in the applications where power consumption is a limiting factor. The power electronics was developed for this system, and an effective relay-based controller was designed which resulted in an optimal closed-loop performance. To date, the linear magnetostrictive motor in the local three-phase operation mode demonstrated its force-generating capability of 410 N and a travel range of 45 mm with a power consumption of 95 W.

Acknowledgment

We would like to thank Prof. Toliyat and Dr. Talebi of Texas A&M University for their invaluable advices on power electronics and magnetic circuit design. We also thank Mr. Young Ha Kim for assistance in fabrication of mechanical parts.

References

[1] I. Boldea and S. A. Nasar, "Linear electric actuators and generators," *IEEE Trans. Energy Conversion*, vol. 14, no. 3, pp. 712–716, Sept. 1999.

[2] H. Ishihara, F. Arai, and T. Fukuda, "Micro mechatronics and micro actuators," *IEEE Trans. Mechatronics*, vol. 1, no. 1, pp. 68–79, March 1996.

[3] J. A. Palmer, B. Dessent, J. F. Mulling, T. Usher, E. Grant, J. W. Eischen, A. I. Kingon, and P. D. Franzon, "The design and characterization of a novel piezoelectric transducer-based linear motor," *IEEE Trans. Mechatronics*, vol. 9, no. 2, pp. 392–398, June 2004.

[4] F. Claeyssen, N. Lhermet, and T. Maillard, "Magnetostrictive actuators compared to piezoelectric actuators," in *Proc. SPIE Conf. Smart Structures in Engineering and Technology*, vol. 4763, 2003, pp. 194–200.

[5] F. Claeyssen, N. Lhermet, R. L. Letty, and P. Bouchilloux, "Acuators, transducers and motors based on giant magnetostrictive materials," *J. Alloys and Compounds*, vol. 258, pp. 61–73, August 1997.

[6] L. Kvarnsjo, "Underwater acoustic transducers based on Terfnenol-D," *J. Alloys and Compounds*, vol. 258, pp. 123–125, August 1997.

[7] L. Kiesewetter, "The application of Terfenol in linear motors," in *Proc. 2nd Int. Conf. Giant Magnetostrictive Alloys*, ch. 7, 1988, p. 15.

[8] W.-J. Kim, J. H. Goldie, M. J. Gerver, J. E. Kiley, and J. R. Swenbeck, "Extended-range linear magnetostrictive motor with double-sided three-phase stators," *IEEE Trans. Industry Applications*, vol. 38, no. 3, pp. 651–659, June 2002.

[9] D. Kendall, and A. R. Piercy, "The frequency dependence of eddy current losses in Terfenol-D," *J. Applied Physics*, vol. 73, pp. 6174–6176, May 1993.

[10] J. Goldie, M. J. Gerver, J. Kiley, and J. R. Swenbeck, "Observations and theory of Terfenol-D inchworm motors," in *Proc. SPIE 5th Annu. Int. Symp. Smart Structures and Materials*, vol. 3329, March 1998, pp. 780–785.

[11] F. Claeyssen, R. L. Letty, N. Lhermet, R. Bossut, and B. Hamonic, "Analysis of magnetostrictive inchworm motors using finite element modeling," in *Proc. Elsevier Conference Magnetoelastic Effects and Applications*, Holland, 1993, pp. 161–167.

[12] M. E. H. Benbouzid, G. Reyne, and G. Meunier, "Finite element modeling of magnetostrictive devices: investigations for the design of the magnetic circuit," *IEEE Trans. Magnetics*, vol. 31, no. 3, pp. 1813–1816, May 1995.

[13] G. Engdahl, *Handbook of Giant Magnetostrictive Materials.* CA: Academic Press, 2000.

[14] Y. Z. Tsypkin, *Relay Control Systems.* Cambridge: Cambridge University Press, 1984.